MATERIALS CHEMISTRY
FRONTIERS

CCS 中国化学会 CHINESE CHEMICAL SOCIETY
ICCAS
ROYAL SOCIETY OF CHEMISTRY

RESEARCH ARTICLE

View Article Online
View Journal | View Issue

Cite this: *Mater. Chem. Front.*, 2024, **8**, 3166

Construction of excellent solid-state electrolyte by incorporating Li-IL into open-pore MOF/polymer-based materials†

Zhi-Peng Ren, [a] Bowei Cong, [a] Feixue Xu, [a] Shuyue Ouyang,[b] Jia-Hui Zhao,[b] Hao-Jie Yang,[b] Shaohui Guo, [a] Dongzheng Wu,[b] Xiaochuan Duan *[ac] and Xian-Ming Zhang *[ac]

Metal–organic framework (MOF)/polymer-based composites are frequently utilized in solid-state electrolytes because of because of the high interfacial compatibility of polymers and the ion-screening ability of MOFs. They are alse often combined with ionic liquids (ILs) to form composite solid-state electrolytes (CSEs). However, the conventional method of combining these components sacrifices some of their individual excellent properties. In this work, the HKUST-1 (Cu) and polyacrylonitrile (PAN) polymer were efficiently combined to create pore-exposed HKUST-1/PAN fibers. Subsequently, the Li-IL@HKUST-1/PAN CSE was obtained by introducing ILs containing lithium salt (Li-IL) into the pores of HKUST-1. At 25 °C, the synthesized CSE exhibited an ionic conductivity of 2.40 × 10^{-3} S cm^{-1} and a lithium-ion mobility number of 0.698. Furthermore, this CSE enables the assembly of $LiFePO_4$/Li solid-state batteries with outstanding cycling performance and multiplicity ranging from 0.1C to 5C at room temperature, with a stable reversible capacity of 67.5 mA h g^{-1} after 100 cycles at a high current density of 5C (25 °C) with a capacity retention of 94.1%. The electrochemical performance of Li-IL@HKUST-1/PAN is significantly superior to that of the conventional Li-IL/HKUST-1/PAN, which can be attributed to the effective combination of HKUST-1, PAN and Li-IL. This combination allows each component to fully exhibit its advantages and synergistically enhances the overall performance, facilitating the selective and rapid transport of lithium ions. This study presents new opportunities for multi-component composite solid-state electrolytes with high performance.

Received 27th May 2024,
Accepted 17th July 2024

DOI: 10.1039/d4qm00436a

rsc.li/frontiers-materials

1. Introduction

Solid-state electrolyte (SSE) assisted high energy density and high safety performance are the most promising directions for the development of next-generation lithium batteries,[1–3] but the current performance of SSE often fails to meet application requirements,[4,5] and further improvements in their high ionic conductivity and interfacial compatibility are necessary. Metal–organic frameworks (MOFs) are porous materials formed by combining metal ions and organic ligands, which have high porosity, large specific surface area, and good stability, making them useful in various fields.[6] Introducing MOFs into the field of SSE[7] also shows numerous advantages due to these characteristics, including direct contact with other components, ion diffusion pathways, modulation of active centers, anion restriction, and impurity capture.[8] MOFs offer additional pathways for lithium-ions (Li^+) diffusion due to their abundant pores, promoting lithium transport and uniform deposition, inhibiting the growth of lithium dendrites,[9] and significantly enhancing the safety performance of the battery. However, the application of MOFs in SSE presents several unavoidable challenges, including complex preparation and molding processes,[10] susceptibility to framework collapse when pressed into an electrolyte film,[11] high impedance and poor compatibility at the electrode contact interface,[12] and susceptibility to agglomeration. To meet the requirements of SSE applications, composite solid-state electrolytes (CSEs) are created by combining MOFs with polymers and/or ionic liquids (ILs) to enhance overall performance.

MOFs have been extensively studied as SSEs by combining them with polymers.[13–16] In this approach, MOFs are used as fillers to enhance the room-temperature performance of the polymers and as ionic mobility pathways to facilitate ionic

[a] *Key Laboratory of Interface Science and Engineering in Advanced Materials Ministry of Education, Taiyuan University of Technology, Taiyuan 030024, China*
[b] *College of Chemical Engineering and Technology, Taiyuan University of Technology, Taiyuan 030024, China. E-mail: zhangxianming@tyut.edu.cn, duanxiaochuan@tyut.edu.cn*
[c] *College of Chemistry, Taiyuan University of Technology, Taiyuan 030024, China*

† Electronic supplementary information (ESI) available. See DOI: https://doi.org/10.1039/d4qm00436a

transport, for example, Mg-MOFs have been doped into PEO by Mathew.[16] However, the polymer tends to clog the pores of MOFs during compounding and it is difficult to utilize their excellent porous properties, as well as the shortcomings of uneven distribution of MOFs and insufficient room-temperature ionic conductivity, which have limited their practical applications.[17,18]

The emergence of *in situ* grown MOF–polymer fibers[19–22] follow with the exploration of MOF complexes while avoiding the agglomeration of MOFs and retains the microporosity of MOFs. This enables the unique properties of both MOFs and polymers to be fully utilized.[23] Unfortunately, the room temperature ionic conductivity of MOF–polymer composite systems still struggles to meet the requirements of SSE applications.[9]

In order to further enhance the room temperature ionic conductivity of the SSE of MOFs system, MOFs were combined with ILs as Li-IL@MOF.[24,25] The frame-structured MOFs host allows ILs to maintain their benefits (high ionic conductivity), while avoiding the risk of leakage due to strong microporous absorption.[26] ILs of room-temperature molten salts as guests enhance room temperature ionic conductivity and interfacial properties.[26] For example, Wang and co-workers[27] introduced ILs into MOF-525(Cu), the solid–solid contact interface between the solid electrolyte and the electrode was optimized as a kind of nano-wetting interface, which resulted in a better interfacial compatibility between the solid electrolyte and the electrode. Meanwhile the nanoconfinement in microporous of MOFs affect the phase behavior of ILs,[28] and exhibit higher ionic conductivity at low temperatures. In addition, its open metal site (OMS) can effectively anchor the anions and allow only the cations to pass through,[29–31] which greatly improves the selectivity of Li^+ and can effectively remove the ionic gradient, and effectively inhibit the growth of lithium dendrites.

Herein, we have prepared HKUST-1/PAN composite fibers with uniform distribution of HKUST-1 and the pores not blocked by the guest by the modified one-pot coaxial electrospinning method, and then introduced Li-IL into the pores of HKUST-1 to obtain Li-IL@HKUST-1/PAN CSE, the preparation principle and scheme are shown in Fig. 1 and Fig. S2 (ESI†). The open pores of HKUST-1 can adsorb Li-IL more efficiently, enabling the preparation of CSEs with higher ionic conductivity and interfacial compatibility, and its OMS can restrict anions to enhance the selectivity of the electrolyte for Li^+. This structural design allows MOFs, polymers and ILs to combine efficiently, effectively combining the advantages of both *in situ* grown MOF–polymers and IL@MOF systems, exploiting the advantages of each component while avoiding the disadvantages, for better overall performance while simplifying the preparation process.

As a result, the prepared Li-IL@HKUST-1/PAN CSE, with an ionic conductivity of 2.40×10^{-3} S cm^{-1} and a lithium-ion mobility number of 0.698 at 25 °C, has superior electrochemical performance to Li-IL/HKUST-1/PAN with conventional pore-plugging MOF–polymer fibers inefficiently blended with Li-IL. In addition, the $LiFePO_4$/Li solid state battery assembled with this CSE has good multiplicity and cycling performance at various current densities (0.1C, 0.2C, 0.5C, 1C, 2C and 5C), with a capacity of 149.9 mA h g^{-1} after 160 cycles at 0.1C, 144.9 mA h g^{-1} after 100 cycles at 0.2C, 125.4 mA h g^{-1} after 55 cycles at 0.5C, 122.4 mA h g^{-1} after 150 cycles at 1C, 106.7 mA h g^{-1} after 100 cycles at 2C and 67.5 mA h g^{-1} after 100 cycles at 5C.

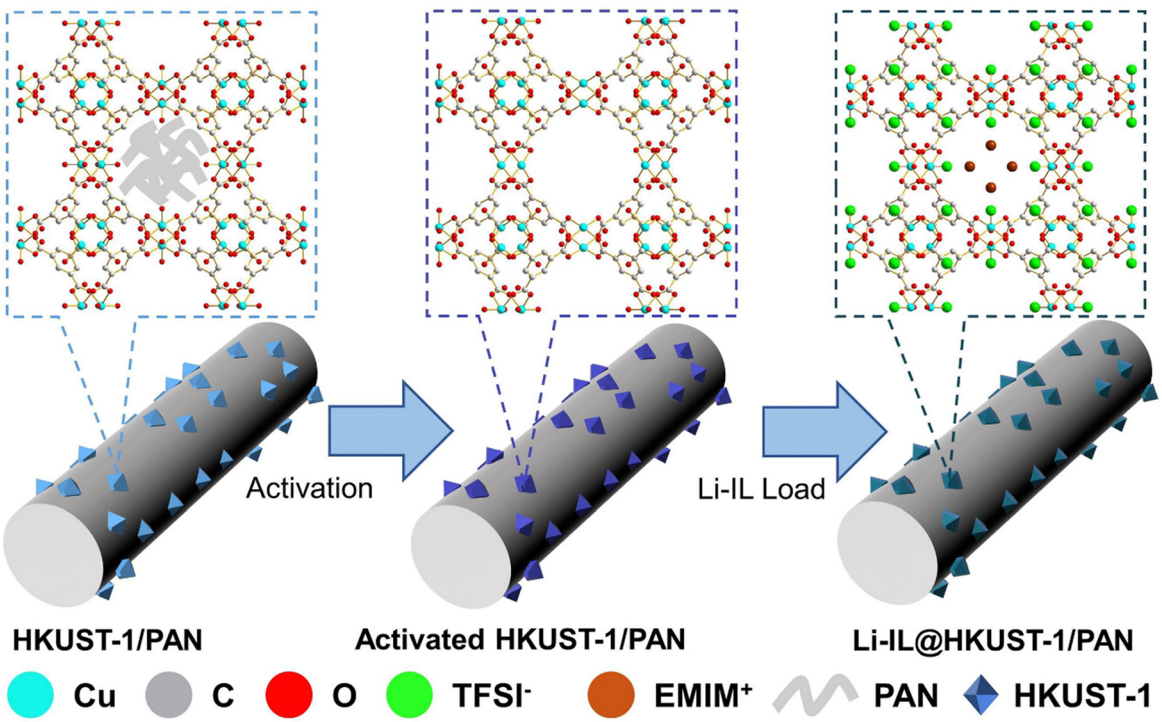

Fig. 1 Schematic of the efficient combination of HKUST-1, PAN and Li-IL into Li-IL@HKUST-1/PAN CSE.

2. Experiment

2.1 Preparation of HKUST-1/PAN

The HKUST-1/PAN membrane was prepared using a one-pot coaxial electrospinning strategy modified from the one-pot electrospinning method.[32,33] Firstly, 0.192 g H_3BTC was dissolved into a mixture of 4 mL DMF/DMSO (volume ratio 1 : 1), and at the same time of slow stirring, 0.4 g PAN was dissolved into the solution, which was used as the coaxial electrospinning core layer electrospinning solution after magnetic stirring at 60 °C for 3 h. Then, 0.204 g $Cu(NO_3)_2{\cdot}3H_2O$ was dissolved into a mixture of 2 mL DMF/DMSO (volume ratio 1 : 1), which was magnetically stirred for 30 min and used as a coaxial electrospinning solution for the shell layer of electrospinning. The core electrospinning solution and shell electrospinning solution were respectively loaded into 5 mL plastic syringes and coaxial electrospinning was carried out with a voltage of 19 kV, the advancing speed of the core and shell solution was 0.4 mL h^{-1} and 0.2 mL h^{-1} respectively, the spinning time was 10 h, and the distance between the tip and the collector was 15 cm. The pristine composite fibers membrane of light blue color HKUST-1/PAN were prepared using the one-pot coaxial electrospinning strategy.

2.2 Activation of HKUST-1/PAN membrane

The light blue fibers membrane obtained by coaxial electrospinning was washed with methanol to remove the HKUST-1 precursor, and then soaked in methanol solution for 12 h, and the methanol solution was replaced every 2 h to fully remove the residual object in the MOF channel, and finally vacuumed at 100 °C for 5 h. Purple HKUST-1/PAN composite fibers membrane with MOF channels open was obtained.

2.3 Preparation of Li-IL@HKUST-1/PAN CSE

Firstly the activated HKUST-1/PAN composite membrane was stamped into 16 mm discs. Then bis(trifluoromethane) sulfonamide lithium (LiTFSI) was dissolved in the ionic liquid 1-ethyl-3-methylimidazolium bis(trifluoromethane) sulfonamide ($[EMIM^+]$ $[TFSI^-]$) mixed as Li-IL ($[EMIM_{0.8}$ $Li_{0.2}{}^+]$ $[TFSI^-]$) in a molar ratio of 2 : 8. Finally, the activated HKUST-1/PAN discs were immersed in Li-IL, and then vacuum dried at 100 °C to obtain dark blue Li-IL@HKUST-1/PAN composite solid electrolyte. All the above operations were carried out in an argon atmosphere glove box (O_2 and $H_2O \leq 0.01$ ppm).

2.4 Preparation of Li-IL/HKUST-1/PAN CSE

Li-IL/HKUST-1/PAN CSE prepared from conventional pore-clogging MOF–polymer fibers inefficiently blended with Li-IL is similar to the preparation of Li-IL@HKUST-1/PAN. 0.408 g $Cu(NO_3)_2{\cdot}3H_2O$ was dissolved into a mixture of 4 mL DMF/DMSO, and 0.4 g PAN was dissolved into the solution, which was used as the coaxial electrospinning core layer solution after stirring at 60 °C for 3 h. And 0.096 g H_3BTC was dissolved into a mixture of 2 mL DMF/DMSO, used as a coaxial electrospinning solution for the shell layer. The coaxial electrospinning was carried out with a voltage of 19 kV, the advancing speed of the core and shell solution was 0.4 mL h^{-1} and 0.2 mL h^{-1} respectively, and the distance was 15 cm. After washing and drying with methanol to remove the residues, conventional pore-clogging MOF–polymer fibers membrane was obtained. Sliced into 16 mm discs and immersed in Li-IL for a period of time, then dried to obtain Li-IL/HKUST-1/PAN CSE.

3. Results and discussion

3.1 Li-IL@HKUST-1/PAN characterisations

As shown in Fig. 2(a) and (b), the original HKUST-1/PAN is light blue and turns purple after solvent-exchange vacuum activation. This corresponds to the complete removal of the guest in HKUST-1 and the revealing of the open metal site (OMS). These results prove that the MOF pores in the HKUST-1/PAN composite fibers are not blocked by the polymer. The one-pot coaxial electrospinning has successfully prepared MOF-open porous HKUST-1/PAN fibrous membrane. The HKUST-1/PAN fibrous membrane turned dark blue as Fig. 2(c) upon loading Li-IL into the HKUST-1 pore channels, consistent with the color change reported in the literature for Li-IL@HKUST-1 activation and loading.[30,31] This suggests successful loading of Li-IL into the HKUST-1/PAN fibers with open pore channels. Fig. 2(d), (e) and Fig. S1a (ESI†) are the SEM and the corresponding EDS mapping images before loading of Li-IL on HKUST-1/PAN. Fig. 2(f), (g) and Fig. S1b (ESI†) are the SEM and EDS images after loading of Li-IL on HKUST-1/PAN. It's evident that Li-IL is successfully encapsulated within the MOF and uniformly distributed on the fiber surface.

Then HKUST-1/PAN and Li-IL@HKUST-1/PAN were subjected to a series of characterisations. Fig. 3(a) shows the XRD of the composite fibers before and after Li-IL loading, both of the samples correspond to the standard HKUST-1. This indicates

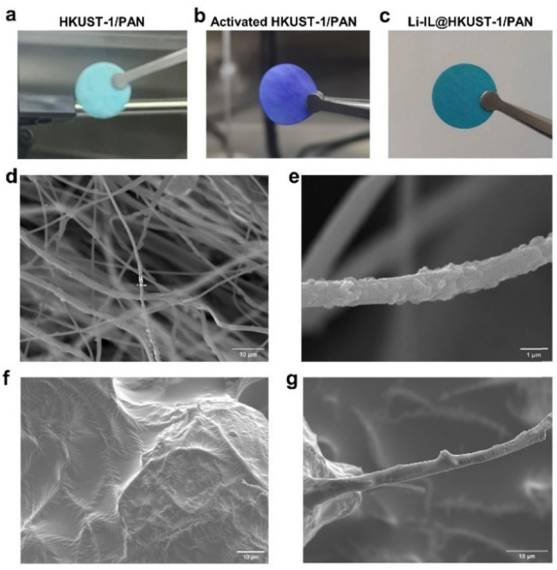

Fig. 2 Image of open porositied HKUST-1/PAN: (a) before activation, (b) after activation, (c) after Li-IL loading, and SEMs of HKUST-1/PAN (d) and (e) and Li-IL@HKUST-1/PAN (f) and (g).

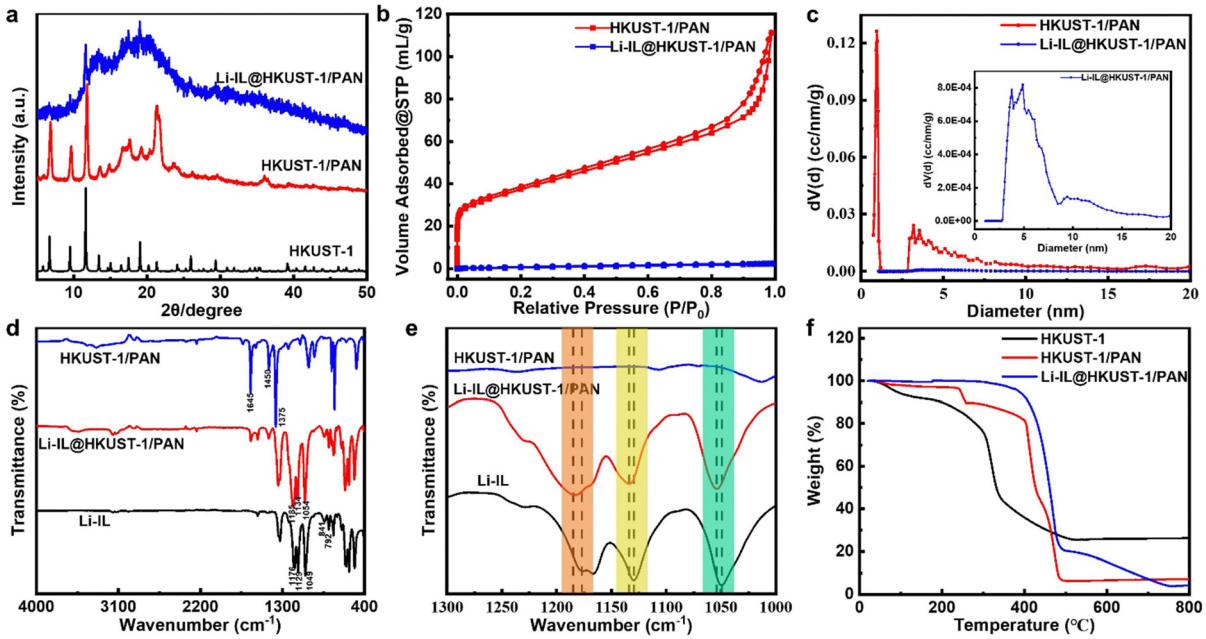

Fig. 3 Characterizations of HKUST-1/PAN and Li-IL@HKUST-1/PAN: (a) XRD, (b) BET nitrogen adsorption and desorption curve, (c) corresponding pore size distribution, (d) FT-IR, (e) locally amplified FT-IR, and (f) TGA curve.

that the one-pot coaxial electrospinning method successfully prepared HKUST-1/PAN, and the framework structure of the MOF was not destroyed after the loading of Li-IL, but rather that it entered the pore channels of the MOF as a guest. The decrease in crystallinity of Li-IL@HKUST-1/PAN after loading may be attributed to the presence of amorphous Li-IL. This weakens the characteristic peaks of the MOF crystals and enhances the bulge peaks of the polymer corresponding to Li-IL.[34] The addition of Li-IL further reduces the crystallinity of the electrolyte, contributing to the improvement of the room temperature ionic conductivity of the composite polymer solid-state electrolyte. Fig. 3(b) displays the N_2 adsorption and desorption curve before and after Li-IL loading. It is evident that HKUST-1/PAN has a significantly higher N_2 adsorption amount than Li-IL@HKUST-1/PAN. Meanwhile, Fig. 3(c) shows that the pore size distribution of HKUST-1/PAN is concentrated around 0.9 nm, consistent with the pore structure of HKUST-1 in the literature.[30] This allows Li^+ (0.076 nm), $EMIM^+$ (0.79 nm), and $TFSI^-$ (0.76 nm) to enter the 3D pores of HKUST-1. However, the pore size distribution of Li-IL@HKUST-1/PAN disappears in the vicinity of 0.9 nm. All these indicate that Li-IL has successfully occupied the pore of HKUST-1. Then the interaction between Li-IL and HKUST-1 channel was further characterized by FT-IR. Fig. 3(d) and (e) shows the FT-IR of Li-IL, HKUST-1/PAN and Li-IL@HKUST-1/PAN. The peaks in the 1700–1300 cm^{-1} region correspond to the carboxylic acid group of the H_3BTC ligand. The peaks at 1645 cm^{-1} are associated with asymmetric telescoping vibrations of the ligand's carboxylic acid group, while the peaks at 1450 and 1375 cm^{-1} are associated with symmetric telescoping vibrations of the same group.

The infrared spectra of Li-IL@HKUST-1/PAN show new characteristic peaks at 792, 841, 1054, 1134, and 1185 cm^{-1} compared to the infrared spectra of HKUST-1/PAN. These peaks correspond to the S–N, C–H, S–N–S, S═O, and C–F functional groups of Li-IL, respectively, indicating successful loading of Li-IL. The infrared spectra of Li-IL show characteristic peaks of S–N, C–H, S–N–S, S═O, and C–F functional groups at 792, 841, 1049, 1129, and 1176 cm^{-1}, respectively. It has been observed that certain characteristic peaks of Li-IL shift after loading onto HKUST-1/PAN. Specifically, the S–N–S functional group shifts from 1049 cm^{-1} to 1054 cm^{-1}, the S═O functional group shifts from 1129 cm^{-1} to 1134 cm^{-1}, and the C–F functional group shifts from 1176 cm^{-1} to 1185 cm^{-1}. The peak characteristic of the anionic $TFSI^-$ functional group is shifted to higher wave numbers, indicating synergistic coordination between the OMS Cu^{2+} of HKUST-1 and $TFSI^-$ due to electrostatic interactions. This results in the immobilisation of $TFSI^-$ by HKUST-1 in Li-IL@HKUST-1/PAN electrolyte. This statement is consistent with the XRD and BET characterization of Li-IL@HKUST-1/PAN.

The thermal stability of CSE was investigated before and after Li-IL loading. Fig. 3(f) shows the thermal decomposition curves of HKUST-1, HKUST-1/PAN, and Li-IL@HKUST-1/PAN. HKUST-1 exhibits two distinct weight loss zones: the removal of guests, such as H_2O, from the MOF pore occurs at near 100 °C, while the collapse and decomposition of the framework structure occurs at near 300 °C. HKUST-1/PAN exhibits two distinct weight loss zones: the epoxidation dehydrogenation reaction of PAN pre-oxidation at around 220 °C and the pyrolytic carbonation of MOF and PAN at approximately 400 °C. Li-IL@HKUST-1/PAN exhibits two significant weight loss regions, with a sharp mass loss of 79.02 wt% near 400 °C, which is mainly due to the thermal decomposition of Li-IL and MOF, and a weight loss percentage of 16.69 wt% from 500 to 800 °C, which is due to the carbonation decomposition of PAN. Therefore, it can

be inferred that HKUST-1 account for 28.38 wt% in HKUST-1/PAN, HKUST-1 and Li-IL accounts for 16.36 wt% and 42.35 wt% respectively in Li-IL@HKUST-1/PAN. Meanwhile, the thermal decomposition temperature of Li-IL@HKUST-1/PAN is higher than that of the single component, with more excellent thermal stability. The results suggest that the combination of HKUST-1, PAN, and Li-IL can enhance the thermal stability of CSE.

3.2 Li-IL@HKUST-1/PAN CSE properties

To verify the enhancement effect of introducing MOF and ILs into polymer solid state electrolyte, a series of tests on the electrochemical performance of Li-IL@HKUST-1/PAN CSE state electrolyte which efficient composite of HKUST-1, PAN, and Li-IL, were carried out. Fig. 4(a) displays the EIS pattern of a CSE-assembled steel-sheet (ss) symmetric cell. The cell has a thickness of 120 μm, an intrinsic impedance of 2.49 Ω, and a room temperature ionic conductivity of 2.40×10^{-3} S cm^{-1}, which is considerably higher than that of conventional Li-IL/HKUST-1/PAN (8.32×10^{-4} S cm^{-1}) (Fig. S3, ESI†). The ionic conductivity of the CSE increases with the temperature increases. Fig. S4 (ESI†) displays the Arrhenius curve of CSE from 25 °C to 55 °C. The fitting of the curve yields an activation energy of 0.21 eV, indicating that Li^+ conduction is dependent on the pore and electrostatic interactions of MOF and Li-IL. Then, in order to ascertain whether the enhanced performance is attributable to interfacial or bulk conduction, Li-IL was further loaded onto the surface or inside of HKUST-1/PAN by dropping or soaking to improve the interfacial or bulk Li^+ conduction. Fig. S5 (ESI†) illustrates the ionic conductivity and interfacial impedance of CSE after soaking (1.08×10^{-3} S cm^{-1}, 281.6 Ω) to improve the bulk conduction was superior to that after dropping (8.64×10^{-4} S cm^{-1}, 399.2 Ω) to improve the interfacial conduction. This further demonstrates that loading Li-IL inside MOF to improve the bulk conduction of Li^+ can lead to the electrochemical performance of Li-IL@HKUST-1/PAN exceeding that of conventional Li-IL/HKUST-1/PAN. This conduction is not limited by the slow relaxation motion of the polymer, which is consistent with the high room temperature ionic conductivity of CSE.

Fig. 4(b) illustrates the impedance changes before and after constant potential polarization of CSE-assembled lithium symmetric batteries. The high internal lithium-ion mobility of CSE reaches 0.698, which is significantly higher than that of the conventional Li-IL/HKUST-/PAN (0.17) (Fig. S3, ESI†). This is attributed to the fact that the OMS of HKUST-1 anchors the anionic limiting domains of Li-IL to only allow cations to participate in the ionic conduction, which greatly enhances the selectivity of CSE for Li^+, and is conducive to the inhibition of lithium dendrite growth and lithium uniform deposition, which is also consistent with the FT-IR characterization of the CSE in Fig. 3(d) and (e).

In addition, we indirectly controlled the Li-IL loading by modifying the loadable pores of HKUST-1/PAN to probe the effect of Li-IL content. As illustrated in Fig. S6 (ESI†), the 0.9 nm loadable Li-IL pores of the partially activated HKUST-1/PAN are obstructed, and the resulting 0.75 nm pores are challenging to load Li-IL, resulting in a substantial gas adsorption but a diminished loading of Li-IL. The performance of the resulting

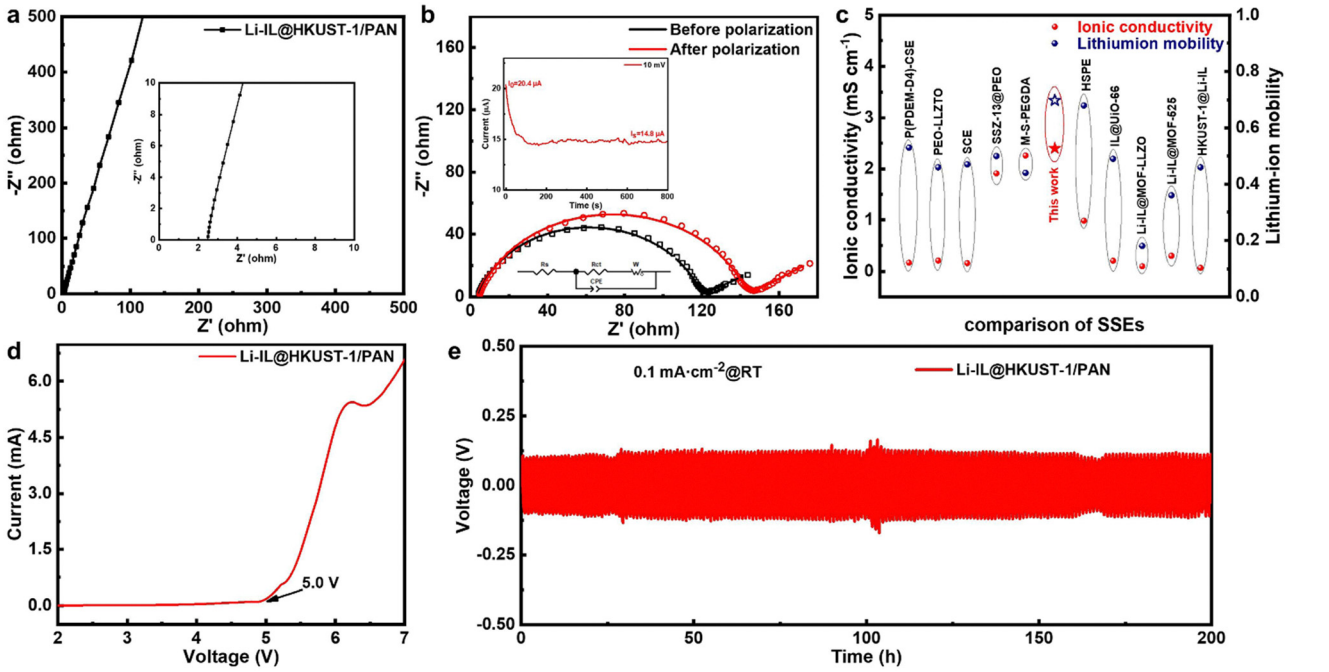

Fig. 4 Properties of HKUST-1/PAN and Li-IL@HKUST-1/PAN: (a) AC impedance mapping of steel-sheet (ss) symmetric cells, (b) AC impedance mapping before and after constant voltage polarization of CSE (internal constant current polarization curve and equivalent circuit diagram), (c) ionic conductivities and lithium-ion mobility of Li-IL@HKUST-1/PAN CSE in comparison with different representative electrolytes, (d) LSV curves for Li||CSE||ss, (e) constant current density charge/discharge cycles for Li||CSE||Li.

partially activated loaded CSE (1.79×10^{-3} S cm^{-1}, 0.31) is also considerably inferior to that of the fully activated CSE (2.40×10^{-3} S cm^{-1}, 0.698). High loading of Li-IL favours CSE performance.

The ionic conductivities and t_{Li+} for Li-IL@HKUST-1/PAN CSE are compared to those reported for SSEs and shown in Fig. 4(c) and Table S1 (ESI†). These include polymeric SSE: P(PDEM-D4)-CSE (1.68×10^{-4} S cm^{-1}, 0.53 at 60 °C);[35] and ceramic SSEs: PEO-LLZTO (2.1×10^{-4} S cm^{-1}, 0.46 at 30 °C),[36] SCE (1.6×10^{-4} S cm^{-1}, 0.47 at 30 °C);[37] and MOF-based polymeric SSEs: SSZ-13@PEO (1.91×10^{-3} S cm^{-1}, 0.5 at 60 °C),[38] M-S-PEGDA (2.26×10^{-3} S cm^{-1}, 0.44 at 30 °C),[39] HSPE (9.83×10^{-4} S cm^{-1}, 0.68 at 60 °C);[40] and IL-loading MOF-based solid-state electrolytes: IL@UiO-66 (2.06×10^{-4} S cm^{-1}, 0.49 at 60 °C),[41] Li-IL@MOF-LLZO (1.0×10^{-4} S cm^{-1}, 0.18 at 60 °C),[29] Li-IL@MOF-525 (3.0×10^{-4} S cm^{-1}, 0.36 at 60 °C),[27] HKUST-1@Li-IL (0.68×10^{-4} S cm^{-1}, 0.46 at 60 °C).[30] Compared with these reported SSEs, our Li-IL@HKUST-1/PAN CSE have excellent ionic conductivities (2.40×10^{-3} S cm^{-1}) and high lithium-ion mobility (0.698) at room temperatures.

The DC polarization (LSV) curve in Fig. 4(d) characterised the electrochemical stability window of CSE. Electrochemical decomposition of CSE did not occur until 5.0 V, indicating that the CSE meets the requirements for solid-state electrolyte applications. Furthermore, the performance of the battery's electrolyte/electrode interface was characterised. The CSE has good chemical stability for lithium metal (Fig. S7, ESI†), interfacial impedance becomes stable after 7 h. As depicted in Fig. 4(e), The lithium-symmetric battery of CSE was cycled stably for 200 hours at room temperature with a current density of 0.1 mA cm^{-2} and an overpotential of approximately 120 mV, demonstrating excellent interfacial compatibility. This could beattributed to the wetting of the interface with Li-IL, which reduced the interfacial impedance and lowered the polarization.

3.3 Solid-state batteries electrochemical performance

To test the electrochemical properties of the as-prepared CSE state electrolyte, $LiFePO_4$ and Li were used as the positive and negative electrodes, respectively. A button-type solid-state lithium battery was assembled using Li-IL@HKUST-1/PAN or Li-IL/HKUST-1/PAN as the solid electrolyte for electrochemical performance testing. As Fig. 5(a) shows the cycling performance of these two batteries at different multiplicities. The Li-IL@HKUST-1/PAN battery has high reversible specific capacities at 0.2C, 0.5C, 1C, 2C, 5C and 10C, which are 150.2 mA h g^{-1}, 141.3 mA h g^{-1}, 129.2 mA h g^{-1}, 110.8 mA h g^{-1}, 84.4 mA h g^{-1} and 60.3 mA h g^{-1}, respectively, whereas when the current multiplicity is drastically decreased from 10C to 0.2C, the

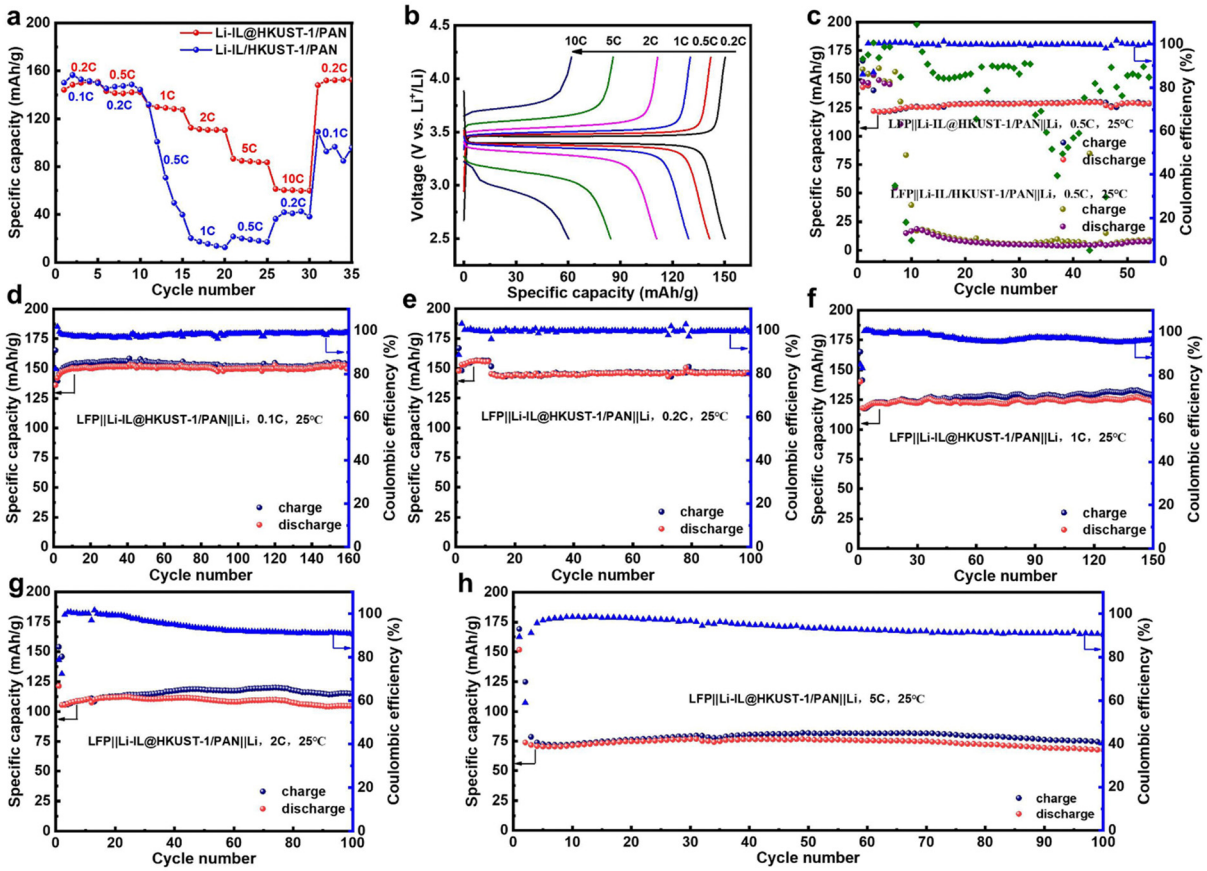

Fig. 5 Electrochemical properties of Li-IL@HKUST-1/PAN at 25 °C: (a) different rate cycle curve, (b) different rate charge and discharge curve, (c) 0.5C long cycle, (d) 0.1C long cycle, (e) 0.2C long cycle, (f) 1C long cycle, (g) 2C long cycle, (h) 5C long cycle.

battery capacity can still be recovered to 148.2 mA h g^{-1}, with a capacity retention rate of about 98.7%. This corresponds to the charging and discharging curves at different multiplicities in Fig. 5(b). The cell polarization increases with increasing cell multiplicity, while the charging plateau increases and the discharging plateau decreases. However, the high specific capacity is still maintained at the high 5C multiplicity. This statement demonstrates that the Li-IL@HKUST-1/PAN solid electrolyte exhibits favourable interfacial compatibility with the electrode and exceptional multiplication performance. In contrast, Li-IL/HKUST-1/PAN battery suffer severe capacity degradation at 0.5C, and even if the current multiplication rate is subsequently reduced to 0.1C, the battery capacity can only be restored to around 90 mA h g^{-1}.

Furthermore, the battery's long-term performance was tested at various rates. As depicted in Fig. 5(c), the graph illustrates these two batteries' long cycle performance at 0.5C. The initial stable capacity of Li-IL@HKUST-1/PAN battery after activation was 130.1 mA h g^{-1}, and the capacity after 55 cycles at 0.5C was 125.4 mA h g^{-1}, with a capacity retention rate of 96.4%. In contrast, Li-IL/HKUST-1/PAN battery had a dramatic drop in capacity after activation. It is further demonstrated that the electrochemical performance of Li-IL@HKUST-1/PAN CSE with open MOF pores efficiently combined with Li-IL is much better than that of Li-IL/HKUST-1/PAN CSE with conventional MOF pores blocked and simply mixed with Li-IL.

Then, Li-IL@HKUST-1/PAN battery's long-term performance was tested at 0.1C, 0.2C, 1C, 2C and 5C. As depicted in Fig. 5(d), the graph illustrates the battery's long cycle performance at 0.1C, its initial stable capacity after activation is 154.3 mA h g^{-1}, and the capacity after 160 cycles at 0.1C is 149.9 mA h g^{-1}, with capacity retention rate of 97.4%. At the same time, the charge and discharge curves of different cycles except for the first circle are highly overlapping (Fig. S8, ESI†). This further proves that the electrolyte is stable at 0.1C. Fig. 5(e) illustrates the battery's performance at 0.2C, its initial capacity is 145.4 mA h g^{-1}, and 144.9 mA h g^{-1} after 100 cycles, with a capacity retention rate of 99.7%. Fig. 5(f) illustrates the performance at 1C, with the initial of 125.8 mA h g^{-1}, and 122.4 mA h g^{-1} after 150 cycles, with a capacity retention rate of 97.3%. Fig. 5(g) illustrates the performance at 2C, with the initial of 110.6 mA h g^{-1}, and 106.7 mA h g^{-1} after 100 cycles, with a capacity retention rate of 96.5%. Fig. 5(h) illustrates the performance at 5C, with the initial of 71.7 mA h g^{-1}, and 67.5 mA h g^{-1} after 100 cycles, with a capacity retention rate of 94.1%. In summary, the electrochemical properties of Li-IL@HKUST-1/PAN solid state electrolytes are demonstrably superior to those of Li-IL/HKUST-1/PAN, maintaining high specific capacity and long cycle stability at 0.1C, 0.2C, 0.5C, 1C, 2C and 5C.

4. Conclusions

In conclusion, a one-pot coaxial electrospinning method was used to rapidly prepare HKUST-1/PAN composite fibrous membrane with open pores. Li-ILs were introduced into the HKUST-1 pores, utilizing the micropores and open metal site (OMS) of HKUST-1 to anchor the anions in Li-IL in the restrictive domain while allowing only the cations to pass through. This achieved an efficient combination of HKUST-1, ILs, and PANs. The Li-IL@HKUST-1/PAN solid-state electrolyte prepared in this study demonstrates excellent performance, with a room temperature ionic conductivity of 2.40 × 10^{-3} S cm^{-1}, an activation energy of 0.21 eV, and a lithium-ion mobility number of 0.698. The Li-IL@HKUST-1/PAN all-solid-state battery exhibits good multiplicity and cycling performance at various current densities (0.1C, 0.2C, 0.5C, 1C, 2C and 5C). The aforementioned results demonstrate that Li-IL@HKUST-1/PAN exhibits superior performance compared to conventional Li-IL/HKUST-1/PAN, and is more suitable for solid-state batteries. Above all, it can be concluded that the combination strategy of HKUST-1, ILs, and PAN presented in this paper offers a new direction for developing high-performance solid-state electrolytes with multi-system composites.

Author contributions

Zhi-Peng Ren performed all the experiments and the data analyses as well as wrote the manuscript; Xian-Ming Zhang and Xiaochuan Duan were in charge of this scientific research project, and the leaders of actual coordination of contributions. All authors contributed to the general discussion.

Data availability

The data supporting this article have been included as part of the ESI.†

Conflicts of interest

There are no conflicts to declare.

Acknowledgements

This work was financially supported by the National Natural Science Foundation of China (grant no. 22271211) and the Natural Science Foundation of Shanxi Province (grant no. 20210302123107 and 202202060301018).

References

1 C. Li, Y. Huang, X. Liu, C. Chen, X. Feng, Z. Zhang and P. Liu, Composite solid electrolyte with Li^+ conducting 3D porous garnet-type framework for all-solid-state lithium batteries, *Mater. Chem. Front.*, 2022, **6**, 1672–1680.
2 L. Tian, J.-W. Kim and D.-W. Kim, Solid hybrid electrolytes based on conductive oxides and polymer electrolytes for all-solid-lithium batteries, *Mater. Chem. Front.*, 2024, **8**, 455–484.
3 P. Wei, H. Wang, M. Yang, J. Wang and D. Wang, Relocatable Hollow Multishelled Structure-Based Membrane Enables Dendrite-Free Lithium Deposition for Ultrastable

Lithium Metal Batteries, *Adv. Energy Mater.*, 2024, **14**, 2400108.
4 S. Lou, F. Zhang, C. Fu, M. Chen, Y. Ma, G. Yin and J. Wang, Interface Issues and Challenges in All-Solid-State Batteries: Lithium, Sodium, and Beyond, *Adv. Mater.*, 2020, **33**, 200721.
5 L. Liu, D. Zhang, X. Xu, Z. Liu and J. Liu, Challenges and Development of Composite Solid Electrolytes for All-solid-state Lithium Batteries, *Chem. Res. Chin. Univ.*, 2021, **37**, 210–231.
6 H. Wang, Q.-L. Zhu, R. Zou and Q. Xu, Metal–Organic Frameworks for Energy Applications, *Chem*, 2017, **2**, 52–80.
7 T. Chen, S. Chen, Y. Chen, M. Zhao, D. Losic and S. Zhang, Metal–organic frameworks containing solid-state electrolytes for lithium metal batteries and beyond, *Mater. Chem. Front.*, 2021, **5**, 1771–1794.
8 E. M. Miner and M. Dinca, Metal- and covalent–organic frameworks as solid-state electrolytes for metal-ion batteries, *Philos. Trans. R. Soc., A*, 2019, **377**, 20180225.
9 S. Bai, Y. Sun, J. Yi, Y. He, Y. Qiao and H. Zhou, High-Power Li-Metal Anode Enabled by Metal–Organic Framework Modified Electrolyte, *Joule*, 2018, **2**, 2117–2132.
10 H. Li, M. Liu, W. Zou, Y. Lv, Y. Liu and L. Chen, Selective Hydrodeoxygenation of Lignin and Its Derivatives without Initial Reaction Pressure Using MOF-Derived Carbon-Supported Nickel Composites, *ACS Sustainable Chem. Eng.*, 2022, **10**, 5430–5440.
11 S. Yuan, X. Sun, J. Pang, C. Lollar, J.-S. Qin, Z. Perry, E. Joseph, X. Wang, Y. Fang, M. Bosch, D. Sun, D. Liu and H.-C. Zhou, PCN-250 under Pressure: Sequential Phase Transformation and the Implications for MOF Densification, *Joule*, 2017, **1**, 806–815.
12 A. Baktash, J. C. Reid, Q. Yuan, T. Roman and D. J. Searles, Shaping the Future of Solid-State Electrolytes through Computational Modeling, *Adv. Mater.*, 2020, **32**, e1908041.
13 W. Hou, Y. Ou and K. Liu, Progress on High Voltage PEO-based Polymer Solid Electrolytes in Lithium Batteries, *Chem. Res. Chin. Univ.*, 2022, **38**, 735–743.
14 S. Mu, Z. Bi, S. Gao and X. Guo, Combination of Organic and Inorganic Electrolytes for Composite Membranes Toward Applicable Solid Lithium Batteries, *Chem. Res. Chin. Univ.*, 2021, **37**, 246–253.
15 M. Zhu, J. Wu, W.-H. Zhong, J. Lan, G. Sui and X. Yang, A Biobased Composite Gel Polymer Electrolyte with Functions of Lithium Dendrites Suppressing and Manganese Ions Trapping, *Adv. Energy Mater.*, 2018, **8**, 1702561.
16 D. E. Mathew, S. Gopi, M. Kathiresan, A. M. Stephan and S. Thomas, Influence of MOF ligands on the electrochemical and interfacial properties of PEO-based electrolytes for all-solid- state lithium batteries, *Electrochim. Acta*, 2019, **319**, 189–200.
17 W. Lei, H. Li, Y. Tang and H. Shao, Progress and perspectives on electrospinning techniques for solid-state lithium batteries, *Carbon Energy*, 2022, **4**, 539–575.
18 M. Wang, Y. Wu, M. Qiu, X. Li, C. Li, R. Li, J. He, G. Lin, Q. Qian, Z. Wen, X. Li, Z. Wang, Q. Chen, Q. Chen, J. Lee, Y.-W. Mai and Y. Chen, Research progress in electrospinning engineering for all-solid-state electrolytes of lithium metal batteries, *J. Energy Chem.*, 2021, **61**, 253–268.
19 Y.-n Wu, F. Li, H. Liu, W. Zhu, M. Teng, Y. Jiang, W. Li, D. Xu, D. He, P. Hannam and G. Li, Electrospun fibrous mats as skeletons to produce free-standing MOF membranes, *J. Mater. Chem.*, 2012, **22**, 16971–16978.
20 H. Liang, X. Jiao, C. Li and D. Chen, Flexible self-supported metal–organic framework mats with exceptionally high porosity for enhanced separation and catalysis, *J. Mater. Chem. A*, 2018, **6**, 334–341.
21 C. Liu, Y. N. Wu, C. Morlay, Y. Gu, B. Gebremariam, X. Yuan and F. Li, General Deposition of Metal–Organic Frameworks on Highly Adaptive Organic–Inorganic Hybrid Electrospun Fibrous Substrates, *ACS Appl. Mater. Interfaces*, 2016, **8**, 2552–2561.
22 Y. Bian, R. Wang, S. Wang, C. Yao, W. Ren, C. Chen and L. Zhang, Metal–organic framework-based nanofiber filters for effective indoor air quality control, *J. Mater. Chem. A*, 2018, **6**, 15807–15814.
23 C. Liao, L. Han, N. Wu, X. Mu, Y. Hu, Y. Kan and L. Song, Fabrication of a necklace-like fiber separator by the electrospinning technique for high electrochemical performance and safe lithium metal batteries, *Mater. Chem. Front.*, 2021, **5**, 5033–5043.
24 M. Urgoiti-Rodriguez, S. Vaquero-Vilchez, A. Mirandona-Olaeta, R. Fernandez de Luis, E. Goikolea, C. M. Costa, S. Lanceros-Mendez, A. Fidalgo-Marijuan and I. Ruiz de Larramendi, Exploring ionic liquid-laden metal–organic framework composite materials as hybrid electrolytes in metal (ion) batteries, *Front. Chem.*, 2022, **10**, 995063.
25 F. P. Kinik, A. Uzun and S. Keskin, Ionic Liquid/Metal–Organic Framework Composites: From Synthesis to Applications, *ChemSusChem*, 2017, **10**, 2842–2863.
26 J. C. Barbosa, D. M. Correia, R. Gonçalves, V. de Zea Bermudez, S. Lanceros-Mendez and C. M. Costa, Ionic liquids in the scope of lithium-ion batteries: from current separator membranes to next generation sustainable solid polymer electrolytes, *Mater. Chem. Front.*, 2023, **7**, 5046–5062.
27 Z. Wang, R. Tan, H. Wang, L. Yang, J. Hu, H. Chen and F. Pan, A Metal–Organic-Framework-Based Electrolyte with Nanowetted Interfaces for High-Energy-Density Solid-State Lithium Battery, *Adv. Mater.*, 2018, **30**, 1704436.
28 Y. Yoshida, K. Fujie, D. W. Lim, R. Ikeda and H. Kitagawa, Superionic Conduction over a Wide Temperature Range in a Metal–Organic Framework Impregnated with Ionic Liquids, *Angew. Chem., Int. Ed.*, 2019, **58**, 10909–10913.
29 Z. Wang, Z. Wang, L. Yang, H. Wang, Y. Song, L. Han, K. Yang, J. Hu, H. Chen and F. Pan, Boosting interfacial Li^+ transport with a MOF-based ionic conductor for solid-state batteries, *Nano Energy*, 2018, **49**, 580–587.
30 Z. Wang, H. Zhou, C. Meng, W. Xiong, Y. Cai, P. Hu, H. Pang and A. Yuan, Enhancing Ion Transport: Function of Ionic Liquid Decorated MOFs in Polymer Electrolytes for All-Solid-State Lithium Batteries, *ACS Appl. Energy Mater.*, 2020, **3**, 4265–4274.

31 M. Li, T. Chen, S. Song, Y. Li and J. Bae, HKUST-1@IL-Li Solid-state Electrolyte with 3D Ionic Channels and Enhanced Fast Li^+ Transport for Lithium Metal Batteries at High Temperature, *Nanomaterials*, 2021, **11**, 736.

32 C. C. Chen, W. D. Zhang, H. Zhu, B. G. Li, Y. Y. Lu and S. P. Zhu, Fabrication of metal–organic framework-based nanofibrous separator via one-pot electrospinning strategy, *Nano Res.*, 2021, **14**, 1465–1470.

33 K. Xue, Y. Si, S. Xie, J. Yang, Y. Mo, B. Long, W. Wei, P. Cao, H. Wei, H. Guan, E. G. Michaelis, G. Guo, Y. Yue and C. Shan, Free-Standing N-Doped Porous Carbon Fiber Membrane Derived From Zn-MOF-74: Synthesis and Application as Anode for Sodium-Ion Battery With an Excellent Performance, *Front. Chem.*, 2021, **9**, 647545.

34 K. Fujie, T. Yamada, R. Ikeda and H. Kitagawa, Introduction of an ionic liquid into the micropores of a metal–organic framework and its anomalous phase behavior, *Angew. Chem., Int. Ed.*, 2014, **53**, 11302–11305.

35 Q. Wang, T. Dong, Q. Zhou, Z. Cui, X. Shangguan, C. Lu, Z. Lv, K. Chen, L. Huang, H. Zhang and G. Cui, An in-situ generated composite solid-state electrolyte towards high-voltage lithium metal batteries, *Sci. China: Chem.*, 2022, **65**, 934–942.

36 J. Zhang, N. Zhao, M. Zhang, Y. Li, P. K. Chu, X. Guo, Z. Di, X. Wang and H. Li, Flexible and ion-conducting membrane electrolytes for solid-state lithium batteries: Dispersion of garnet nanoparticles in insulating polyethylene oxide, *Nano Energy*, 2016, **28**, 447–454.

37 H. Huo, Y. Chen, J. Luo, X. Yang, X. Guo and X. Sun, Rational Design of Hierarchical ''Ceramic-in-Polymer'' and ''Polymer-in-Ceramic'' Electrolytes for Dendrite-Free Solid-State Batteries, *Adv. Energy Mater.*, 2019, **9**, 1804004.

38 W. Li, S. Zhang, B. Wang, S. Gu, D. Xu, J. Wang, C. Chen and Z. Wen, Nanoporous Adsorption Effect on Alteration of the Li^+ Diffusion Pathway by a Highly Ordered Porous Electrolyte Additive for High-Rate All-Solid-State Lithium Metal Batteries, *ACS Appl. Mater. Interfaces*, 2018, **10**, 23874–23882.

39 H. Wang, Q. Wang, X. Cao, Y. He, K. Wu, J. Yang, H. Zhou, W. Liu and X. Sun, Thiol-Branched Solid Polymer Electrolyte Featuring High Strength, Toughness, and Lithium Ionic Conductivity for Lithium-Metal Batteries, *Adv. Mater.*, 2020, **32**, e2001259.

40 K. Pan, L. Zhang, W. Qian, X. Wu, K. Dong, H. Zhang and S. Zhang, A Flexible Ceramic/Polymer Hybrid Solid Electrolyte for Solid-State Lithium Metal Batteries, *Adv. Mater.*, 2020, **32**, e2000399.

41 H. Niu, N. Zhang, M. Ding, T. Hou, D. Zhang, L. Wang, P. Guan and X. Hu, Preparation of poly(ionic liquid) composite quasi-solid electrolyte by incorporating metal–organic framework filler decorated with ionic liquid for lithium batteries, *Solid State Ionics*, 2022, **380**, 115945.

